Journal of
Materials Chemistry A

PAPER

Cite this: J. Mater. Chem. A, 2017, 5, 19390

# Pressure-induced abnormal insulating state in triangular layered cobaltite $Li_xCoO_2$ ($x = 0.9$)†

Cong Xu,[‡a] Weiji Xiao,[‡b] Tongchao Liu,[‡b] Fei Sun,[ac] Jiaxin Zheng,[b] Shang Peng,[a] Xuqiang Liu,[a] Feng Pan,[*b] Wenge Yang[*ac] and Ho-kwang Mao[abd]

Received 13th July 2017
Accepted 21st August 2017

DOI: 10.1039/c7ta06084j

rsc.li/materials-a

Lithium cobaltite oxides ($Li_xCoO_2$) have been serving as an important rechargeable battery material with reversible extraction and insertion of lithium ions. During the charge–discharge process, 50% or more amount of lithium can be extracted, and the layered structure remains stable with a semiconductor to metal transition at around $x = 0.7$. Static high pressure, an effective tool to tune crystal and electronic structure, is utilized herein in the most studied layered compound $Li_{0.9}CoO_2$ to investigate the effects on the structural stability and transport properties by synchrotron X-ray diffraction (XRD), electric resistivity, UV-vis absorption spectroscopy, and *ab initio* calculations. Up to 19.8 GPa, no structural phase transition was observed, but surprisingly its electric transport behavior changed from a semiconducting state to an insulating state. The detailed XRD and UV-vis spectroscopy analysis reveals that the pressure-induced Co–O bond length shrinkage in the $CoO_6$ octahedron enhances crystal field splitting, which leads to band gap opening, and the decrease in Co–Co distance causes the $t_{2g}$ bands to overlap and the electron holes to be localized. The profoundly different response of the ground state to high pressure indicates an unusual, delicate interplay between the crystal structure and the electronic structure in $Li_xCoO_2$ and may provide a new route for the development of lithium-ion battery with high performance under the assistance of pressure.

## Introduction

With their high voltage, high energy density and excellent cycling stability, lithium cobaltite oxides ($LiCoO_2$) have widely served as the cathode material for rechargeable lithium-ion batteries (LIBs), stimulating several investigations on the relationship between their structure and properties.[1–4] $Li_xCoO_2$ forms a layered structure with lithium ions inserted between the Co–O layers, where the $CoO_6$ octahedra share their edges and the cobalt ions form a triangular lattice. $Li_xCoO_2$ with a layered $\alpha$-$NaFeO_2$ structure belongs to the rhombohedral system (space group $R\bar{3}m$) and has Co–O layers and interlayers of Li ions that are alternately stacked along the $c$ axis. The Co–O triangular lattice layer consists of edge-sharing $CoO_6$ octahedra. It is believed that most of the physical properties have a strong connection with the electronic structure of the Co–O layers.[5,6] X-ray absorption spectroscopy (XAS) studies[7,8] and angle-resolved photoemission spectroscopy (ARPES) studies[9] on the delithiated $Li_xCoO_2$ ($x < 1$) reveal that Co is in the 3+/4+ mixed valence state. Both $Co^{3+}$ and $Co^{4+}$ ions stay in their low spin configuration $S = 0(t_{2g}^6e_g^0)$ and $S = 1/2(t_{2g}^5e_g^0)$, respectively. The five Co 3d orbitals split into a lower manifold containing three $t_{2g}$ states and a higher manifold containing two $e_g$ states under the octahedral ligand field, and the three $t_{2g}$ orbitals further split into one $a_{1g}$ orbital and two $e'_g$ orbitals under the distorted octahedral field. The ligand field splitting is mainly due to anisotropic hybridization between the Co 3d orbitals and the O 2p orbitals and, therefore, the O 2p components are mixed with the Co 3d states. The electronic band structure of $Li_xCoO_2$ ($x < 1$) shows that the top valence and bottom conduction bands are formed mainly by the hybridized d states of Co and the p states of O, and the Fermi level is located near the top of the Co 3d $t_{2g}$ bands.[10,11] In delithiated samples, extra electron holes are created in the upper $t_{2g}$ valence bands formed by the overlapping $t_{2g}$ orbitals of Co in the $CoO_6$ octahedral sharing edges, which implies that the geometry of the $CoO_6$ octahedron is strongly connected to the band structure around the Fermi level.

---

[a] *Center for High Pressure Science and Technology Advanced Research (HPSTAR), Shanghai 201203, China. E-mail: yangwg@hpstar.ac.cn*

[b] *School of Advanced Materials, Peking University, Shenzhen Graduate School, Shenzhen, 518055, China. E-mail: panfeng@pkusz.edu.cn*

[c] *Beijing National Laboratory for Condensed Matter Physics, Institute of Physics, Chinese Academy of Sciences, Beijing 100190, China*

[d] *High Pressure Synergetic Consortium (HPSynC), Geophysical Laboratory, Carnegie Institution, Argonne, Illinois 60439, USA*

† Electronic supplementary information (ESI) available: Text and figures give details of the sample preparation, ICP-AES results, typical Rietveld refinement results, structure optimization, structure parameters of supercell of $Li_{0.9}CoO_2$ from DFT calculations, distorted parameter $\Delta_d$, calculated band gap under various external pressures with different Hubbard U, high magnification scanning electron micrographs of $Li_{0.9}CoO_2$ before and after high pressure process. See DOI: 10.1039/c7ta06084j

‡ These authors contributed equally to this work.

A fundamental understanding of the complicated relationship between the structural and electronic properties of $Li_xCoO_2$ is needed to improve battery performance because $Li_xCoO_2$ is a reference compound for the entire family of layered materials obtained by the substitution of other metals for cobalt. Earlier investigations of the $Li_xCoO_2$ system showed that the lithium deintercalation process can cause complicated successive crystal phase transitions.[12–14] For $Li_xCoO_2$ with $0.93 \leq x \leq 1$,[14,15] there is a one-phase solid solution domain with a hexagonal structure (Li-rich hex-I); for $0.5 < x < 0.75$, there is another one-phase region (Li-poor hex-II); and for $0.75 \leq x < 0.93$, Li-rich hex-I and Li-poor hex-II phases can coexist, which is attributed to an insulator-metal transition upon Li extraction.[16] These two phases have the same crystal symmetry ($R\bar{3}m$) and only a small variation in the lattice constants, mainly in the $c$ axis.[13] As highlighted by Ménétrier *et al.*,[14] the Li-rich hex-I phase behaves like a semiconductor, while the Li-poor hex-II phase is metallic, implying that an insulator-metal transition occurs at intermediate Li concentrations. Marianetti *et al.*[15] proposed that this insulator-metal transition is a first-order Mott transition due to the impurities-Li vacancy. A monoclinic phase also appears in a narrow range around $x = 0.5$, which can be attributed to an interlab lithium/vacancy ordering. As for the magnetic properties of the $Li_xCoO_2$ system, both Li-rich hex-I and Li-poor hex-II phases show Curie–Weiss behavior.[3,17] Notably, a magnetic anomaly is observed near 175 K at $x = 0.67$.[18] All these observations suggest that $Li_xCoO_2$ exhibits various interesting electronic, magnetic, and thermoelectric properties, depending on the lithium content $x$.[3,17–20]

In this respect, high-pressure can be a very effective and clean tool compared to chemical doping, *e.g.*, modifying the effective bandwidth ($W$) of transition metals by changing the M–O bond length and/or the M–O–M bond angle and thereby tuning the electronic and magnetic properties of materials. High-pressure driven transformations of several other electrode materials have been reported, for example, $Li_xFePO_4$, $Na_xCoO_2$, $V_2O_5$, and $Li[Li_xNi_{1-x}]O_2$.[21–25] As one of the fundamental state parameters, pressure can vary electrochemical properties dramatically compared to the ambient pressure state. Nonetheless, few experimental and theoretical studies have investigated the behavior of layered $Li_xCoO_2$ materials at high pressure thus far. Wang *et al.*[26] compared experimental high-pressure structural and vibrational properties to *ab initio* calculations for pristine $LiCoO_2$ and found that the structure remained layered up to at least 26 GPa at room temperature with a large inhomogeneous compression rate (the $c/a$ ratio decreases by about 5%). To date, less attention has been paid to the electronic properties of $LiCoO_2$, particularly the defective cobaltites $Li_xCoO_2$ ($x < 1$) under pressure.

Herein, we report the effect of pressure on structural and electronic properties of the semiconductor $Li_xCoO_2$ with $x = 0.90$, by synchrotron X-ray diffraction, electric resistivity, UV-vis absorption spectroscopy and first-principles calculations. We found a dramatic increase in electrical resistivity ($\sim$3 orders of magnitude) and blue shift in the UV-vis absorption spectrum with pressure ranging from 1 bar to 19.8 GPa, while the structural symmetry remained unchanged, which is quite unusual. In most correlated oxides, pressure usually broadens the 3d bandwidth and thereby leads to a transition towards a more conducting state.[27–29] The opposite effect observed in this study is unique and is apparently connected with different physical mechanisms. We explain this behavior to be a consequence of larger crystal field splitting induced by the decrease in Co–O bond length and the $t_{2g}$ bands overlapping due to the decrease in Co–Co distance. Our first principles calculations also provide solid support for this interpretation. The findings uncovered by the comprehensive high pressure investigations provide deep insights into the complex relationship of the crystal structure and electronic performance of this important cathode material, which may be useful for guiding the future lithium metal oxides battery to exhibit better performance.

## Experimental

### Sample preparation

The Li-deficient sample $Li_{0.9}CoO_2$ was obtained by a two-step approach. The pure $LiCoO_2$ was first synthesized by a previously established method,[30,31] and then the Li-deintercalated sample was obtained *via* a chemical extraction process from $LiCoO_2$. Chemical delithiation of the $LiCoO_2$ material was achieved by stirring the powder in acetonitrile solutions containing $NO_2BF_4$ oxidizer in excess. The molar ratio of $LiCoO_2$ and $NO_2BF_4$ is 5 : 1 for the preparation of $Li_{0.9}CoO_2$ samples. After 24 h of lithium extraction at room temperature, the $LiCoO_2$ powder was washed with acetonitrile several times, and the solutions were removed by centrifugation. The resulting materials were then dried at 80 °C. The Li content value $x$ was determined by inductively coupled plasma-atomic emission spectrometry (ICP-AES).[26] The results of the Li content determination are in the ESI Part 1.†

### *In situ* high-pressure XRD

The powder sample was pressed into a pellet and loaded into in a Mao–Bell symmetric diamond anvil cell (DAC) with a pair of 300 μm culet diamonds. The rhenium gasket was pre-indented from a thickness of 250 μm to 40 μm and a sample chamber 160 μm in diameter was drilled in the center of the indented area. Silicone oil was used as a nearly hydrostatic pressure-transmitting medium, and small ruby spheres were placed in the sample chamber to monitor the pressure. *In situ* high-pressure X-ray diffraction experiments were performed at the 16BM-D beamline of the High Pressure Collaborative Access Team (HPCAT) at the Advanced Photon Source (APS) of the Argonne National Laboratory (ANL). A focused monochromatic X-ray beam about 4 μm in diameter (fwhm) and wavelength of 0.3100 Å was used for the diffraction experiments. The XRD patterns were collected with a MAR 3450 image plate detector. The two-dimensional diffraction patterns were converted to one-dimensional intensity profile *versus* $2\theta$ data using FIT2D software.[32] The one-dimensional XRD profiles were analyzed with Rietveld refinements using the GSAS + EXPGUI software packages to obtain the lattice parameters and coordinations of all the atoms.[33]

### *In situ* high-pressure electrical measurement

The electrical resistance measurements under high pressure were performed in a DAC using the standard four-probe method with temperature ranging from 300 K to 80 K obtained by cooling with liquid nitrogen. A T301 stainless steel gasket was pre-indented from a thickness of 250 μm to 40 μm and a hole was drilled at the center with a diameter of 260 μm. A fine cubic boron nitride (c-BN) powder was used to cover the gasket to keep the electrode leads insulated from the metallic gasket. The c-BN powder was pressed and further drilled into a central chamber with a diameter of 160 μm, in which the $Li_{0.9}CoO_2$ powder sample was loaded. Platinum foils with a thickness of 5 μm were cut to several microns in width and were used as electrodes. Four platinum leads were arranged to contact the sample in the chamber. Ruby spheres were placed around the sample for pressure calibration.

### *In situ* high-pressure UV-vis absorption spectroscopy

*In situ* high-pressure UV-vis absorption spectroscopy measurements were performed on an UV-vis absorption spectrophotometer with a response time of 1 s. The wavelength ranged from 400 nm to 800 nm. The intercept of the absorption edge onto the energy axis from a plot $(ah\nu)^2$ *versus* photon energy $(h\nu)$ gives a good approximation of the $Li_{0.9}CoO_2$ band gap energy.

### Density functional theory calculations

All calculations were performed using the Vienna Ab-initio Simulation Package (VASP)[34,35] based on a generalized gradient approximation with Hubbard U correction (GGA + U)[36] to the DFT calculations. The PBE[37] exchange correlation and a plane wave representation for the wave-function with a cut-off of 500 eV were used. $Li_{0.9}CoO_2$ calculations were performed with a $2 \times 2 \times 1$ supercell (Fig. 1(c)). The Brillouin zone was sampled by $4 \times 4 \times 2$ special *k*-points using the Monkhorst–Pack scheme[38] for structural optimization and $7 \times 7 \times 3$ for the density of states (DOS) calculation. Because the d orbital plays an important role in transition metals, the U (on-site coulomb term) value for Co-3d was set at 3.32 eV, which is advised by the Materials Project.[39] Ferromagnetically spin-polarized, antiferromagnetically spin-polarized, as well as non-spin-polarized DFT calculations were used to optimize the structures at various values of external pressures. According to the small energy differences between these magnetic structures, we assumed that $Li_{0.9}CoO_2$ was nonmagnetic for our further calculations (Fig. S1, ESI†).

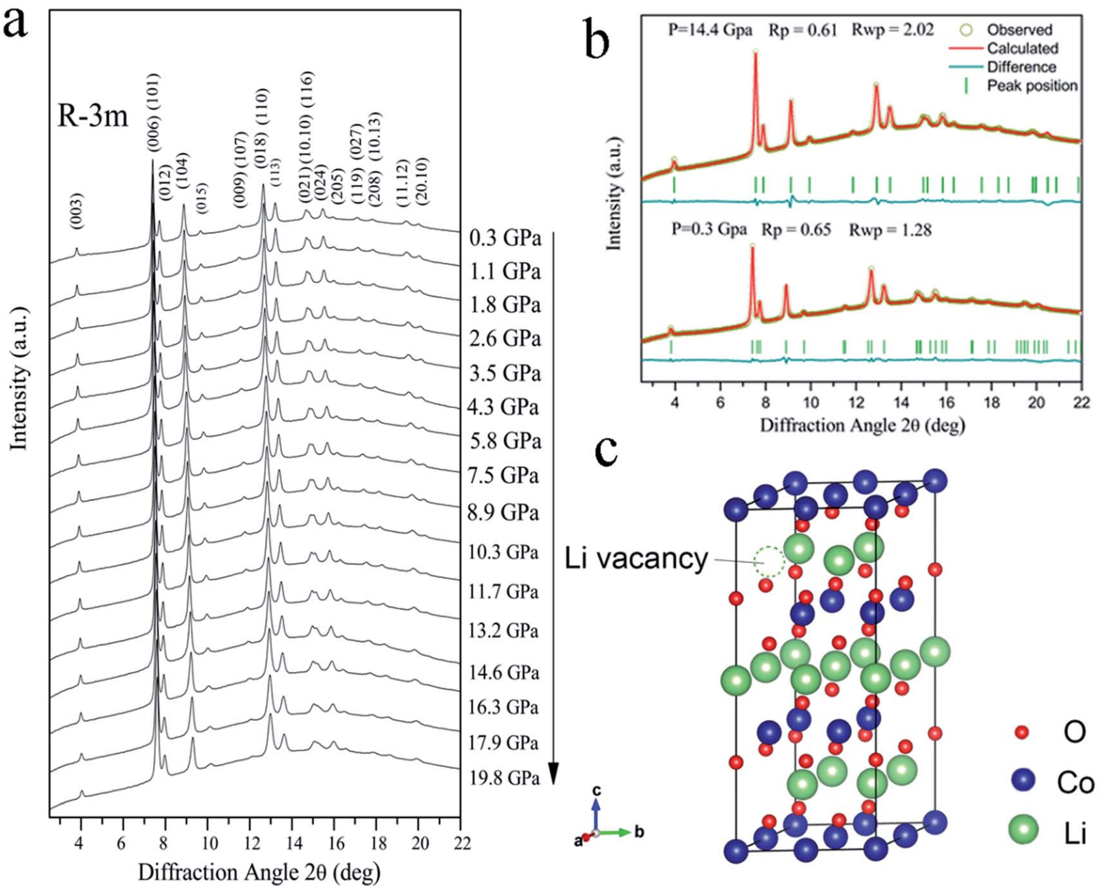

Fig. 1 Crystal structure probed by XRD under pressure up to 20 GPa. (a) Integrated one-dimensional X-ray powder diffraction patterns of $Li_{0.9}CoO_2$ at various pressures and room temperature. The incident X-ray wavelength was $\lambda = 0.3100$ Å. (b) Representative Rietveld refinements for $Li_{0.9}CoO_2$ with $R\bar{3}m$ space group at 0.3 GPa and 14.4 GPa. (c) The atomic model of $2 \times 2 \times 1$ $Li_{0.9}CoO_2$ supercell.

## Results

The powder XRD patterns of $Li_{0.9}CoO_2$ at various high pressures up to 19.8 GPa are presented in Fig. 1(a). In these patterns, no traces of a new phase are observed, and the original hexagonal structure is preserved till the highest pressure herein. No disappearance or splitting/broadening of peaks is observed, indicating that the sample is single phase.[12,14,18] Further detailed investigations were conducted on these XRD patterns with Rietveld refinements to study the atomic positions as a function of pressure. The starting atomic model was based on the pure $LiCoO_2$ structure with space group $R\bar{3}m$. Fig. 1(b) shows the representative Rietveld fittings for $Li_{0.9}CoO_2$ at 0.3 GPa and 14.4 GPa. The weighted residuals of the refinements were $R_{wp} = 1.28\%$ at 0.3 GPa and $R_{wp} = 2.02\%$ at 14.4 GPa. The typical refinement results are summarized in ESI Table 2.†

The pressure dependence of the unit cell parameters of $Li_{0.9}CoO_2$ up to 19.8 GPa based on the Rietveld refinements is shown in Fig. 2(a). The basal lattice parameter $a$ shrinks by 2.7% at 19.8 GPa, whereas $c$ drops by 5.2%, exhibiting large anisotropic compression. Fig. 2(b) shows the volume *versus* pressure plot up to 19.8 GPa. The fitting of the pressure–volume data with the third-order Birch–Murnaghan equation of state[40] yielded the values for the bulk modulus $B_0$ and its pressure derivative $B'_0$ as $B_0 = 159.4(9)$ GPa and $B'_0 = 5.8(4)$. The values of the bulk modulus ($B_0$) and its derivative ($B'_0$) are close to the values of $LiCoO_2$ ($x = 1$) with $B_0 = 149(2)$ GPa and $B'_0 = 4.1(3)$.[26] The obtained value of the ambient pressure unit cell volume $V_0$ was 95.45 $Å^3$.

Fig. 2(c) shows the Co–O bond length as a function of pressure. With increasing pressure, the Co–O bond length decreased. Fig. 2(d) describes the volume compression of the $CoO_6$ octahedron. Upon compression, the Co–O bond length decreased and the interactions between the central Co atom and the O ligands enhanced further, inducing larger crystal field splitting in the $CoO_6$ octahedron. From a structural perspective, the $CoO_6$ octahedron in $Li_{0.9}CoO_2$ distorted as the pressure increased. In the lithium cobaltite oxides family, electrical transport properties have an important connection with the Co–O layers, and hence we expected pressure to have a significant impact on the electronic properties of $Li_{0.9}CoO_2$.

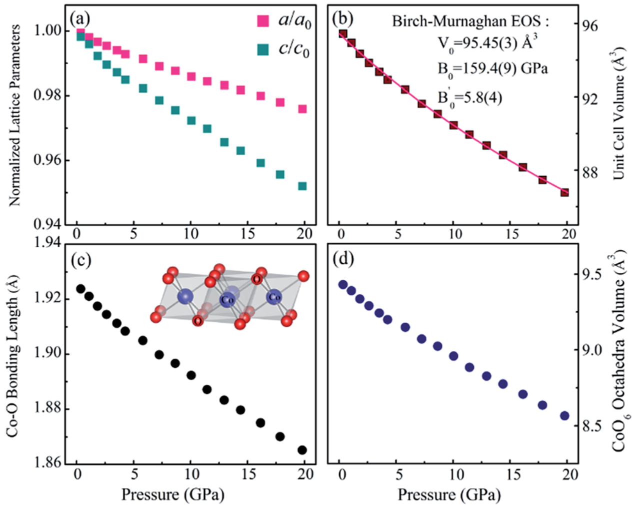

Fig. 2 Structural parameters of $Li_{0.9}CoO_2$ as a function of pressure. (a) Normalized lattice parameters $a$ and $c$ of $Li_{0.9}CoO_2$ as a function of pressure; (b) pressure–volume data (symbols) and fitted Birch–Murnaghan relation (solid line); (c) Co–O bond length *versus* pressure; and (d) volume of the distorted $CoO_6$ octahedra as a function of pressure.

Fig. 3(a) illustrates the temperature dependence of the electrical resistivity $\rho(P,T)$ of $Li_{0.9}CoO_2$ at different pressures up to 15.9 GPa. The data shown in the figure were collected during heating after slowly cooling down to ~80 K in a diamond anvil cell (DAC) using the standard four-probe method. $Li_{0.9}CoO_2$ is reported as a narrow-band semiconductor at ambient pressure in earlier studies.[3] As shown in Fig. 3(a), with increasing pressure to 15.9 GPa, the sample $Li_{0.9}CoO_2$ still exhibited a semiconductor behavior in the measured temperature range with an electrical resistivity ($\rho$) increase of 3 orders of magnitude in the low-temperature region. This means that the electronic charge hopping was significantly reduced with increasing pressure.

As this material belongs to a Li-rich solid solution, the electronic conductivity is thermally activated. We examined the activation energy from the intrinsic region of electrical conductivity ($\sigma$) in a polycrystalline $Li_{0.9}CoO_2$ sample. The $\sigma$ (in Napierian logarithmic coordinate) *vs.* the $1/T$ Arrhenius plot in Fig. 3(b) exhibits a linear region in the high-temperature region. The high-$T$ linear region should be attributed to the intrinsic region of $\sigma$ and can be expressed by $\sigma = \sigma_0 \exp(-E_a/k_BT)$, where $\sigma_0$ is the pre-exponential constant, $k_B$ is the Boltzmann constant, and $E_a$ is the activation energy. The fit at various pressures gives the intrinsic $E_a$ values of $Li_{0.9}CoO_2$ as a function of pressure, which is plotted in the inset of Fig. 3(b), demonstrating that the activation energy value exhibits a nearly linear increase with pressure.

A dramatic increase in electrical resistivity ($\rho$) indicates band gap opening under pressure. To confirm this, we utilized UV-vis absorption spectroscopy to measure the pressure dependence of the bandgap. As a crystalline semiconductor, the optical absorption near the band edge follows the formula $ah\nu = A(h\nu - E_g)^{n/2}$,[41] where $a$, $\nu$, $E_g$ and $A$ are the absorption coefficient, light frequency, band gap, and a constant, respectively. The value $n$ depends on the characteristics of the transition in the semiconductor, *i.e.* $n = 1$ for direct transition or $n = 4$ for indirect transition. For $Li_{0.9}CoO_2$, the value of $n$ is 1. The band gap energy ($E_g$ value) of $Li_{0.9}CoO_2$ can be thus estimated from a plot $(ah\nu)^2$ *versus* photon energy ($h\nu$). The intercept of the plot to the $x$-axis gives a good estimation of the band gap energy.

Fig. 4 displays the band gap result from the UV-vis absorption study with pressures up to 19.1 GPa. (a–f) Give the $(ah\nu)^2$ *versus* photon energy ($h\nu$) of the $Li_{0.9}CoO_2$ powder under pressures from 1.7 GPa to 19.1 GPa at room temperature. The red fitted lines give the corresponding band gap estimation shown in Fig. 4(g). We found that the band gap energy of the $R\bar{3}m$ $Li_{0.9}CoO_2$ blue shifts with an increase in pressure.

The estimated band gap energies of the sample were about 1.29, 1.39, 1.49, 1.53, 1.67, and 1.77 eV for $Li_{0.9}CoO_2$ at room temperature and pressures of 1.7, 7.2, 13.6, 15.6, 18.3, and 19.1 GPa, respectively. This trend is consistent with the electrical

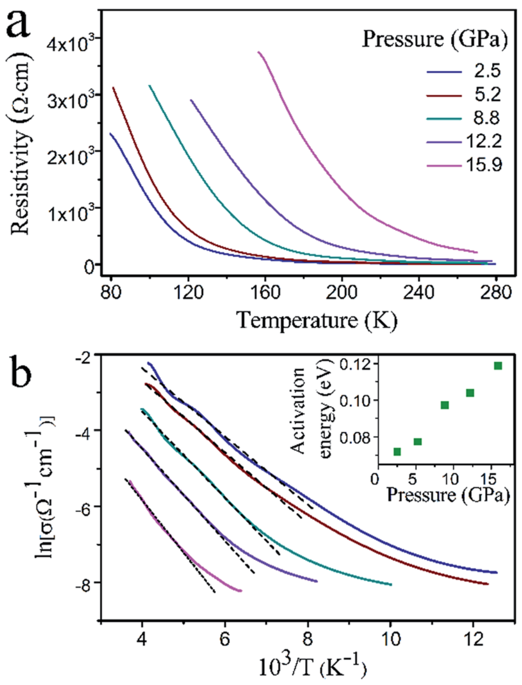

Fig. 3 (a) Temperature dependence of the electrical resistivity $\rho(P,T)$ of $\mathrm{Li_{0.9}CoO_2}$ under different pressures up to 15.9 GPa. (b) Electrical conductivity ln $\sigma$ *versus* $1/T$ curves for the $\mathrm{Li_{0.9}CoO_2}$ sample at various pressures. The dotted lines are the fitted Arrhenius relations at five pressures. The inset shows the activation energy $E_a \sim P$ plot for $\mathrm{Li_{0.9}CoO_2}$ sample.

resistivity increasing by several orders of magnitude with pressure.

Density functional theory (DFT) calculations were also employed for insight into the main experimental results of $\mathrm{Li_{0.9}CoO_2}$. The calculations were extended to volumes corresponding to a pressure of about 40 GPa to see how the structural changes would extrapolate if the layered structure were assumed to be stable over the entire range. Table S3 (ESI†) summarizes the calculated structural parameters of the supercell at various pressures. We can see that both lattice parameters ($a$ and $c$) decrease with increasing external pressure, while the lattice parameter $c$ is more sensitive to pressure variation. At 20 GPa, $c$ shrunk by 5.85% while $a$ dropped by 2.72%, which is in good agreement with our Rietveld refinement results. The average Co–O bond length and $\mathrm{CoO_6}$ octahedral volume also decreased with increasing pressure, consistent with our experiments. To describe the distortion degree of a $\mathrm{CoO_6}$ octahedron, the distortion parameter $\Delta_{\mathrm{d}}$ is defined as $\Delta_{\mathrm{d}} = \frac{1}{6}\sum_{i=1}^{6}\left(\frac{d_i-\bar{d}}{\bar{d}}\right)^2$, where $d_i$ is the length of the $i^{\mathrm{th}}$ Co–O bond and $\bar{d}$ is the average length of all six Co–O bonds inside the octahedron.[42,43] As shown in Table S3 (ESI†), the average $\Delta_{\mathrm{d}}$ is around $3.0 \times 10^{-5}$ and varies little with pressure, thus the decreasing Co–O bond length rather than distortion is responsible for the difference of electronic structure under various pressures. The detailed $\Delta_{\mathrm{d}}$ of all $\mathrm{CoO_6}$ octahedrons in the supercell are shown in Fig. S2, ESI.†

The density of states (DOS) for $\mathrm{Li_xCoO_2}$ under different external pressures is displayed in Fig. 5. The projected density of states (PDOS) of Li is not shown here because the contribution of Li to the valence band and the conduction band is notably very small compared to Co and O. As Fig. 5(a) shows, $\mathrm{LiCoO_2}$ is a band insulator with a Fermi level between the filled $\mathrm{t_{2g}}$ states and the unfilled $\mathrm{e_g}$ states. This result is consistent with the reported literature.[6] As Li is partially removed, the electrostatic potential of the Li vacancy will bind the hole, resulting in an impurity band that breaks away from the top of the valence band.[13,15] Consequently, the Fermi level moves down to across the tail of the valence band and the band gap decreases, which is shown in Fig. 5(b). Therefore, the band gap of the $\mathrm{Li_{0.9}CoO_2}$ is lower than that of $\mathrm{LiCoO_2}$ at ambient pressure. With increased

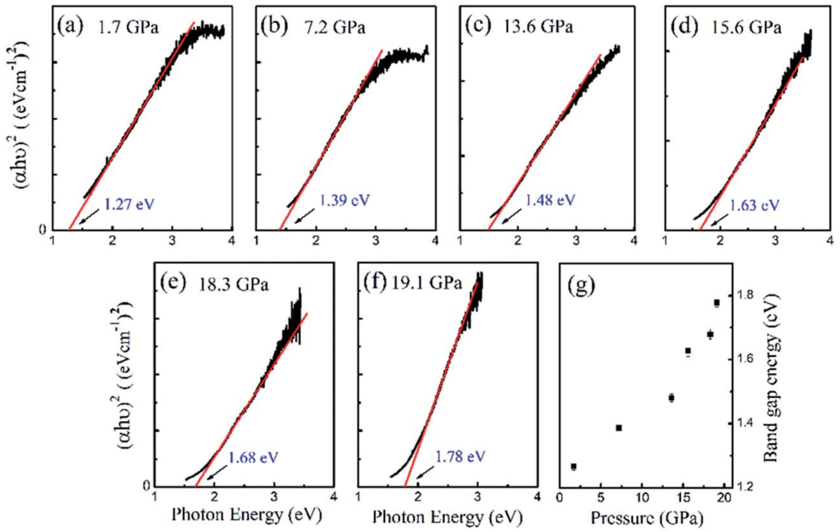

Fig. 4 UV-vis absorption study of the $\mathrm{Li_{0.9}CoO_2}$ band gap under high pressure. (a–f) UV-vis absorption spectra of $\mathrm{Li_{0.9}CoO_2}$ at various pressures from 1.7 GPa to 19.1 GPa. The fitted absorption edges (red lines) provide good estimations of the band gaps. (g) The evolution of the band gap at different pressures from the fitting (a–f).

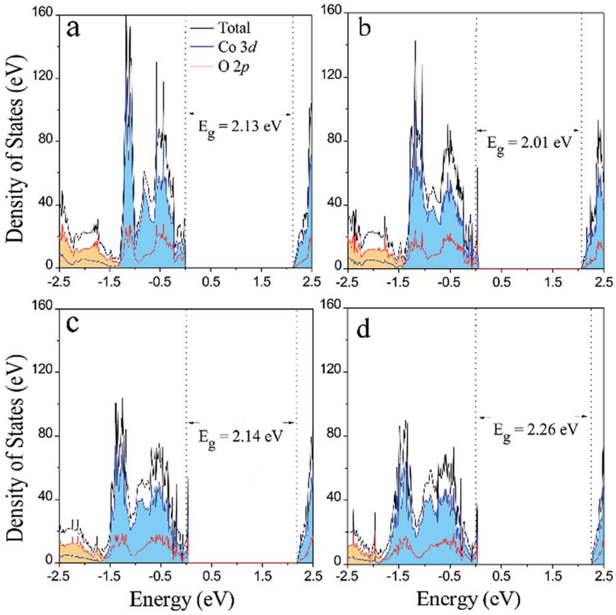

Fig. 5 Density of states (DOS) of $Li_xCoO_2$ (a) $LiCoO_2$ at ambient pressure, (b) $Li_{0.9}CoO_2$ at ambient pressure, and (c) $Li_{0.9}CoO_2$ at 20 GPa (d) $Li_{0.9}CoO_2$ at 40 GPa.

external pressure, the conduction band minimum (CBM) moved up while the valence band maximum (VBM) remained still, leading to the band gap opening shown in Fig. 5(c) and (d), which agrees with the trend from our UV-vis absorption study. It should be noted that the calculated band gap is closely related to the Hubbard U; thus the specific values of the calculated band gap might be quite different from those obtained from experiments. The calculated band gap under various external pressures with different Hubbard U is shown in Fig. S3, ESI.†

To gain further insight into the microscopic origin of the semiconducting to insulating state transition, it is necessary to characterize the difference of the hole at various pressures. As shown in Fig. 6, we plotted the hole density by subtracting the charge density of the partially delithiated structure from that of stoichiometric $LiCoO_2$, while holding all structural parameters constant. The valleys (red) indicate electron accumulation, while the hills (blue) denote electron depletion, *i.e.* hole concentration. It is obvious that the contour lines around the hole move closer on increasing pressure, indicating that the hole becomes more localized. Both the hole localization and band gap opening induced by high pressure contribute towards the insulating state.

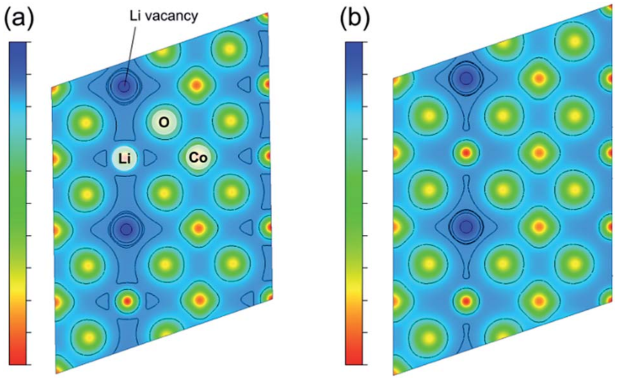

Fig. 6 The total charge-density difference of $Li_{0.9}CoO_2$ with external pressure of (a) 0 GPa and (b) 40 GPa. A plane that cuts through the Co–O octahedral plane is chosen. Units are electrons per Å$^3$.

## Discussion and conclusions

The observation of a strong increase in the electrical resistivity in layered cobalt oxide $Li_{0.9}CoO_2\rho$ (*i.e.*, suppression of electron hopping) on increasing the pressure is unexpected and it opposes the results reported on most TMO. There is no structure phase transition in the investigated pressure range up to 20 GPa. The five Co 3d orbitals split into a lower manifold containing three $t_{2g}$ states and a higher manifold containing two $e_g$ states under the octahedral ligand field, and the three $t_{2g}$ orbitals further split into one $a_{1g}$ orbital and two $e'_g$ orbitals under the distorted octahedral field. Earlier XPS and valence-band UPS studies[6] on the electronic band structure of $Li_xCoO_2$ and our DFT calculations show that the Fermi level is located near the top of the Co 3d $t_{2g}$ bands and the electronic states at the Fermi level are dominated by the $a_{1g}$ band. Our calculations also show that the conduction band minimum (CBM) is dominated by the $e_g$ band. The positions of the $a_{1g}$ and $e_g$ bands can be largely affected by high pressure through a change of the lattice parameter. The length of Co–O bond decrease with increased pressure, which causes the crystal field splitting to increase, *i.e.*, the unoccupied $e_g$ level shift upwards and the $a_{1g}$ level shift downwards; thus the band gap increases. Moreover, the decrease of the Co–Co distance ($d_{Co-Co} = a$) enhance the direct $t_{2g}$–$t_{2g}$ orbital overlapping, ensuring that the electron holes created in the $t_{2g}$ bands are localized. Therefore, under the effect of band gap opening and electron hole localization, the material exhibited a dramatic increase in electrical resistivity. This interpretation is supported by the experimental observation of blue shift in the UV-vis absorbance spectroscopy with increasing pressure.

In summary, we investigated the effect of pressure on the electronic and structural properties of $Li_{0.9}CoO_2$. We observed an abnormal pressure effect: a transition from a semiconducting state to an insulating state, contrary to our original expectations. This finding is a consequence of a pressure-induced crystal field splitting and $t_{2g}$ band overlapping. The pressure-induced semiconducting to insulating state transition was further confirmed by blue shift in the UV-vis absorption spectra and *ab initio* calculations. Our results provide a comprehensive understanding of this type of layered structure material from the lattice, bond length, and electronic configuration perspectives. We expect that the mechanism uncovered here will provide a guideline for finding a strategy to improve lithium ion battery performance.

## Conflicts of interest

There are no conflicts to declare.

## Acknowledgements

This study is supported by the National Natural Science Foundation of China under Grants No. U1530402 and 51527801. Work at Peking University, Shenzhen Graduate School is supported by the National Materials Genome Project (2016YFB0700600), the National Natural Science Foundation of China (No. 21603007), and Guangdong Innovation Team Project (No. 2013N080). Work at Institute of Physics Chinese Academy of Sciences is supported by NSF (Grants No. 11220101003, No. 11534016, and No. 112111KYS820150017), the Ministry of Science & Technology, and Chinese Academy of Sciences of China through Research Projects. The High Pressure Collaborative Access Team operations are supported by DOE-NNSA under Award No. DE-NA0001974 and DOE-BES under Award No. DE-FG02-99ER45775, with partial instrumentation funding by the National Science Foundation. The authors thank Feryja O'Toole, Qian Zhang, Yanping Yang, and Zhipeng Yan for their valuable suggestions and technical support.

## Notes and references

1 H. Abe, K. Zaghib, K. Tatsumi and S. Higuchi, *J. Power Sources*, 1995, **54**, 236–239.

2 M. Pollet, M. Blangero, J.-P. Doumerc, R. Decourt, D. Carlier, C. Denage and C. Delmas, *Inorg. Chem.*, 2009, **48**, 9671–9683.

3 K. Miyoshi, C. Iwai, H. Kondo, M. Miura, S. Nishigori and J. Takeuchi, *Phys. Rev. B: Condens. Matter Mater. Phys.*, 2010, **82**(7), 075113.

4 L. A. Montoro, M. Abbate and J. M. Rosolen, *Electrochem. Solid-State Lett.*, 2000, **3**(9), 410–4112.

5 O. E. Peil, A. Georges and F. Lechermann, *Phys. Rev. Lett.*, 2011, **107**, 236404.

6 K. Ikedo, Y. Wakisaka and T. Mizokawa, *Phys. Rev. B: Condens. Matter Mater. Phys.*, 2010, **82**, 075126.

7 T. Mizokawa, L. H. Tjeng, P. G. Steeneken, N. B. Brookes, I. Tsukada, T. Yamamoto and K. Uchinokura, *Phys. Rev. B: Condens. Matter Mater. Phys.*, 2001, **64**, 115104.

8 T. Mizokawa, L. H. Tjeng, H. J. Lin, C. T. Chen, R. Kitawaki, I. Terasaki, S. Lambert and C. Michel, *Phys. Rev. B: Condens. Matter Mater. Phys.*, 2005, **71**, 193107.

9 M. Hasan, Y. Chuang, D. Qian, Y. Li and Y. Kong, *Phys. Rev. Lett.*, 2004, **92**, 246402.

10 J. van Elp, J. L. Wieland, H. Eskes, P. Kuiper, G. A. Sawatzky, F. M. F. de Groot and T. S. Turner, *Phys. Rev. B: Condens. Matter Mater. Phys.*, 1991, **44**, 6090–6103.

11 K. Ikedo, Y. Wakisaka, T. Mizokawa, C. Iwai, K. Miyoshi and J. Takeuchi, *Phys. Rev. B: Condens. Matter Mater. Phys.*, 2010, **82**, 075126.

12 K. Nakamura, H. Ohno, K. Okamura, Y. Michihiro, T. Moriga, I. Nakabayashi and T. Kanashiro, *Solid State Ionics*, 2006, **177**, 821–826.

13 A. Milewska, K. Świerczek, J. Tobola, F. Boudoire, Y. Hu, D. K. Bora, B. S. Mun, A. Braun and J. Molenda, *Solid State Ionics*, 2014, **263**, 110–118.

14 M. Ménétrier, I. Saadoune, S. Levasseur and C. Delmas, *J. Mater. Chem.*, 1999, **9**, 1135–1140.

15 C. A. Marianetti, G. Kotliar and G. Ceder, *Nat. Mater.*, 2004, **3**, 627–631.

16 J. N. Reimers and J. R. Dahn, *J. Electrochem. Soc.*, 1992, 2091–2097.

17 K. Mukai, Y. Ikedo, H. Nozaki, J. Sugiyama, K. Nishiyama, D. Andreica, A. Amato, P. L. Russo, E. J. Ansaldo, J. H. Brewer, K. H. Chow, K. Ariyoshi and T. Ohzuku, *Phys. Rev. Lett.*, 2007, **99**, 087601.

18 T. Motohashi, T. Ono, Y. Sugimoto, Y. Masubuchi, S. Kikkawa, R. Kanno, M. Karppinen and H. Yamauchi, *Phys. Rev. B: Condens. Matter Mater. Phys.*, 2009, **80**, 165114.

19 J. T. Hertz, Q. Huang, T. McQueen, T. Klimczuk, J. W. G. Bos, L. Viciu and R. J. Cava, *Phys. Rev. B: Condens. Matter Mater. Phys.*, 2008, **77**, 075119.

20 T. Y. Ou-Yang, F. T. Huang, G. J. Shu and W. L. Lee, *Phys. Rev. B: Condens. Matter Mater. Phys.*, 2012, **85**, 035120.

21 S. J. Tracy, L. Mauger, H. J. Tan, J. A. Munoz, Y. Xiao and B. Fultzi, *Phys. Rev. B: Condens. Matter Mater. Phys.*, 2014, **90**, 094303.

22 S. Park, Y. Lee, A. Moodenbaugh and T. Vogt, *Phys. Rev. B: Condens. Matter Mater. Phys.*, 2003, **68**, 180505.

23 F. X. Zhang, S. K. Saxena and C. S. Zha, *J. Solid State Chem.*, 2007, **180**, 1759–1763.

24 I. Loa, A. Grzechnik, U. Schwarz, K. Syassen, M. Hanfland and R. K. Kremer, *J. Alloys Compd.*, 2001, **317–318**, 103–108.

25 E. Shinova, E. Zhecheva, R. Stoyanova, G. D. Bromiley, R. Alcántara and J. L. Tirado, *J. Solid State Chem.*, 2005, **178**, 2692–2700.

26 X. Wang, I. Loa, K. Kunc, K. Syassen and M. Amboage, *Phys. Rev. B: Condens. Matter Mater. Phys.*, 2005, **72**, 224102.

27 Y. Moritomo, A. Asamitsu and Y. Tokura, *Phys. Rev. B: Condens. Matter Mater. Phys.*, 1995, **51**, 16491–16494.

28 I. Loa, P. Adler, A. Grzechnik, K. Syassen, U. Schwarz, M. Hanfland, G. K. Rozenberg, P. Gorodetsky and M. P. Pasternak, *Phys. Rev. Lett.*, 2001, **87**, 125501.

29 C. Meneghini, D. Levy, S. Mobilio, M. Ortolani, M. Nuñez-Reguero, A. Kumar and D. D. Sarma, *Phys. Rev. B: Condens. Matter Mater. Phys.*, 2001, **65**, 012111.

30 Z. H. Wang, X. Y. Chen, M. Zhang and Y. T. Qian, *Solid State Sci.*, 2005, **7**, 13–15.

31 X. L. Xiao, L. M. Yang, H. Zhao, Z. B. Hu and Y. D. Li, *Nano Res.*, 2012, **5**(1), 27–32.

32 A. P. Hammersley, S. O. Svensson, M. Hanfland, A. N. Fitch and D. Hausermann, *High Pressure Res.*, 1996, **14**, 235–248.

33 B. H. Toby, *J. Appl. Crystallogr.*, 2001, **34**, 210–213.

34 G. Kresse and J. Furthmuller, *Phys. Rev. B: Condens. Matter Mater. Phys.*, 1996, **54**, 11169–11186.

35 G. Kresse and J. Furthmuller, *Comput. Mater. Sci.*, 1996, **6**, 15–50.

36 S. L. Dudarev, G. A. Botton, S. Y. Savrasov, C. J. Humphreys and A. P. Sutton, *Phys. Rev. B: Condens. Matter Mater. Phys.*, 1998, **57**, 1505–1509.

37 J. P. Perdew, K. Burke and M. Ernzerhof, *Phys. Rev. Lett.*, 1996, **77**, 3865–3868.

38 H. J. Monkhorst and J. D. Pack, *Phys. Rev. B: Solid State*, 1976, **13**, 5188–5192.

39 A. Jain, S. P. Ong, G. Hautier, W. Chen, W. D. Richards, S. Dacek, S. Cholia, D. Gunter, D. Skinner, G. Ceder and K. A. Persson, *APL Mater.*, 2013, **1**, 011002.

40 F. Birch, *J. Geophys. Res.: Space Phys.*, 1978, **83**, 1257–1268.

41 M. A. Butler, *J. Appl. Phys.*, 1977, **48**, 1914.

42 J. Rodríguez-Carvajal, M. Hennion, F. Moussa and A. H. Moudden, *Phys. Rev. B: Condens. Matter Mater. Phys.*, 1998, **57**, R3189–R3192.

43 J. A. Alonso, M. J. Martınez-Lope, M. T. Casais and M. T. Fernandez-Diaz, *Inorg. Chem.*, 2000, **39**, 917–923.